A Journal of the Gesellschaft Deutscher Chemiker

Angewandte International Edition Chemie

GDCh

www.angewandte.org

Accepted Article

Title: An Activity-Based Sensing Fluorogenic Probe for Monitoring Ethylene in Living Cells and Plants

Authors: Yiliang Chen, Wei Yan, Duojing Guo, Yu Li, Ji Li, Hao Liu, Lirong Wei, Na Yu, Biao Wang, Ying Zheng, Maofeng Jing, Jing Zhao, and Yong-Hao Ye

To be cited as: *Angew. Chem. Int. Ed.* 10.1002/anie.202108335

Link to VoR: https://doi.org/10.1002/anie.202108335

WILEY-VCH

10.1002/anie.202108335

WILEY-VCH

RESEARCH ARTICLE

An Activity-Based Sensing Fluorogenic Probe for Monitoring Ethylene in Living Cells and Plants

Yiliang Chen,[a, b] Wei Yan,[a, b] Duojing Guo,[a, b] Yu Li,[a, b] Ji Li,[c] Hao Liu,[a, b] Lirong Wei,[a] Na Yu,[a, b] Biao Wang,[a, b] Ying Zheng,[a] Maofeng Jing,[a] Jing Zhao,[c] Yonghao Ye*[a, b]

[a] Prof. Dr. Y.H. Ye, Dr. Y.L. Chen, Dr. W. Yan, D.J. Guo, Y. Li, H. Liu, L.R. Wei, Prof. Dr. N. Yu, B. Wang, Y. Zheng, Prof. Dr. M.F. Jing
Key Laboratory of Plant Immunity, College of Plant Protection
Nanjing Agricultural University
Nanjing 210095, P. R. China
E-mail: yeyh@njau.edu.cn

[b] Prof. Dr. Y.H. Ye, Dr. Y.L. Chen, Dr. W. Yan, D.J. Guo, Y. Li, H. Liu, Prof. Dr. N. Yu, B. Wang
State & Local Joint Engineering Research Center of Green Pesticide Invention and Application
Nanjing Agricultural University
Nanjing 210095, P. R. China

[c] Dr. J. Li, Prof. Dr. J. Zhao
State Key Laboratory of Coordination Chemistry, Chemistry and Biomedicine Innovation Center (ChemBIC),
School of Chemistry and Chemical Engineering
Nanjing University
Nanjing 210023, P. R. China

Supporting information for this article is given via a link at the end of the document.

Abstract: Ethylene (ET) is an important gaseous plant hormone. It is highly desirable to develop fluorescent probes for monitoring ethylene in living cells. Herein we report an efficient Rh(III)-catalysed coupling of *N*-phenoxyacetamides to ethylene in the presence of an alcohol. The newly discovered coupling reaction exhibited a wide scope of *N*-phenoxyacetamides and excellent regioselectivity. More importantly, we successfully develop three fluorophore-tagged Rh(III)-based fluorogenic probes (coumarin-ethylene probes, **CEPs**) using this strategy for the selective and quantitative detection of ethylene. Among the probes, **CEP-1** exhibited the highest sensitivity with a limit of detection of ethylene at 52 ppb in air. Furthermore, **CEP-1** was successfully applied for imaging in living CHO-K1 cells and for monitoring endogenous-induced changes in ethylene biosynthesis in tobacco and *Arabidopsis thaliana* plants. These results indicated that **CEP-1** has great potential to illuminate the spatiotemporal regulation of ethylene biosynthesis and ethylene signal transduction in living biological systems.

Introduction

Ethylene (ET) is an important gaseous plant hormone that is involved in a variety of growth and development processes, such as seed germination, cell elongation, fertilization, fruit ripening, and seed dispersal. It also plays important roles in pathogen defence and response to external stress factors.[1] The ethylene biosynthesis pathway has been well established and consists of two main steps: the ethylene precursor SAM (*S*-adenosyl-$_L$-methionine) is first converted to ACC (1-aminocyclopropane-1-carboxylic acid) by ACC synthase (ACS), and then ACC is oxidized by ACC oxidase (ACO) to generate ethylene.[2] The canonical signaling pathway is that ethylene signaling involves ethylene receptors (ETR1, ERS1, ETR2, EIN4, ERS2), the protein kinase CTR1, and EIN2 that signals to the transcription factors EIN3, EIL1, and EIL2. These, in turn, signal to other transcription factors such as the ERFs leading to ethylene responses. Although the ethylene signal transduction pathway has been extensively studied, the biochemical modes of action of many of the signaling components are still unresolved.[3] Therefore, the development of a real-time monitoring method for ethylene is helpful for the insight of ethylene biology. Unfortunately, there are no cost-effective methods available to rapidly quantitate ethylene concentrations.[4] Currently, the primary technologies for ethylene detection include gas chromatography,[5] photoacoustic spectroscopy,[6] and electrochemical methods;[7] however, these technologies usually suffer from high costs or lacking real-time monitoring of ethylene levels.

Fluorescent, especially fluorogenic, metal complexes have been widely applied in complex biomolecule modification and especially useful in detecting ethylene via its coordination or reactivity. Silver(I) and copper(I) can reversibly coordinate ethylene. The pioneering work in Burstyn group described a poly(vinyl phenyl ketone) (PVPK) polymer film that luminesces when coordinated to impregnated silver(I) ions. Upon exposure to ethylene gas, the binding is disrupted, and the silver(I) ion mediates quenching of the PVPK photoluminescence.[8] Later, Swager and colleagues reported an ingenious design of a sensor where the quenching of the fluorescence of a conjugated polymer by copper(I) complexes could be reversed by binding ethylene.[9] Pivotal progress by the Hitomi group described an interesting silver(I)-anthracene complex containing an intramolecular metal-arene interaction, which could be disrupted by exposure to ethylene gas.[10] However, these approaches were not applied in biological systems. *In situ* metabolite imaging by optical methods is becoming increasingly important in chemical biology[11]. Activity-based sensing (ABS), which utilizes molecular reactivity, rather than conventional lock-and-key molecular recognition for analyte detection. Notably, Chang et al. extensively applied this ABS strategy in the selective detection of molecular analytes in complex biological environments, especially on metal-dependent reactivity for bioimaging and related purposes.[12] Recently, tremendous progress was made by Michel,[13] Huang,[14] and Tanaka,[15] who took advantage of the well-known Grubbs catalyst and designed highly sensitive fluorescent probes to detect ethylene

10.1002/anie.202108335

in vivo by olefin-metathesis. These ruthenium-based strategies tremendously improved the potential of the applications in more complex biological systems. Inspired by these previous work, we aim to design a fluorogenic probe for the selective detection of endogenous ethylene with high sensitivity and to explore other metals (besides silver, copper, ruthenium).

In 2014, Zhao group reported Rh(III) catalysed the reaction of *N*-phenoxyacetamides with α,β-unsaturated aldehydes to synthesize 1,2-oxazepines through the activation of C-H/[4 + 3] annulation.[16] Another report from Zhao group indicated that the use of Rh(III) to catalyse the tandem reaction of *N*-phenoxyacetamides and alkynes with multiple functional groups led to structural diversity.[17] In 2017, Zhao group described a Rh(III)-catalysed *ortho*-arylation reaction of *N*-phenoxyacetamides with benzothiazoles to obtain corresponding mono/disubstituted arylated phenol products.[18] These hydrocarbon activation reactions can produce the same intermediate **A**, a Rh(III)-based five-membered ring (Scheme 1), and intermediate **A** could react with various unsaturated hydrocarbons to form the corresponding products. Given that ethylene gas is the simplest alkene, we hypothesized that *N*-phenoxyacetamides could also react with ethylene and carried out exploring experiments to test this hypothesis, which led the discovery of a novel type of ethylene activation reaction. The reaction mechanism indicates that intermediate **A** could couple with ethylene and an alcohol to form new C-H bonds. Inspired by the role of intermediate **A** in the hydrocarbon activation reaction with alkene as the substrate, we designed a fluorophore-tagged rhodium metal complex that might provide a selective and sensitive chemodosimeter for the detection of ethylene. Herein, Rh(III) metal catalysts acted as quenchers to bind coumarin to form the nonfluorescent **CEP** (coumarin-ethylene-probe), and reaction with ethylene gas formed **CEP-ET**, resulting in the fluorescence "turn-on" of coumarin. Coumarin-metal complexes were rationally designed and synthesized as a real-time fluorescent sensor to detect ethylene gas in CHO-K1 cells, tobacco and *Arabidopsis* leaves.

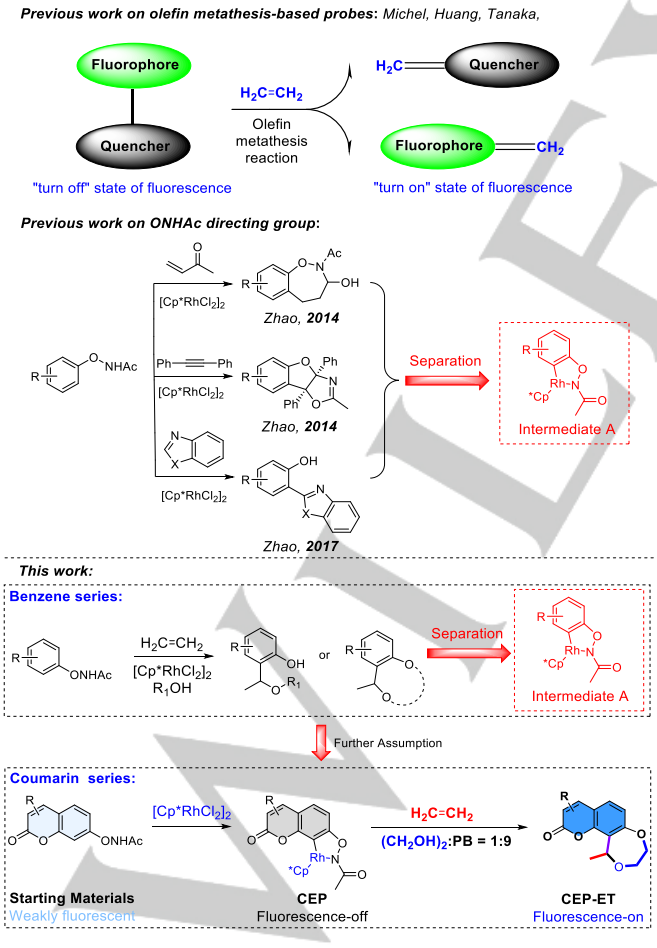

Scheme 1. Design of the fluorogenic detection of ethylene by a Rh(III)-coumarin complex.

Results and Discussion

We first performed optimization experiments on the hydrocarbon activation reaction of *N*-phenoxyacetamide (**1a**) with ethylene. Encouragingly, the treatment of **1a** with ethylene in the presence of $[Cp^*RhCl_2]_2$ (10 mol %) and CsOAc (1.0 equiv) in various alcohols (MeOH, EtOH, *n*-propanol, ethylene glycol) at room temperature for 5 min led to the formation of the catenarian products 2-(1-methoxyethyl)phenol (**2aa**, 87%), 2-(1-ethoxyethyl)phenol (**2ab**, 79%), 2-(1-propoxyethyl)phenol (**2ac**, 83%) and the annulated product 5-methyl-2,3-dihydro-*5H*-benzo[*e*][1,4]dioxepine (**2ad**, 68%) (Table 1, entries 9, 11-13). Compared to $[Cp^*RhCl_2]_2$, other transition metal catalysts, such as iridium, ruthenium, and platinum, are ineffective under current conditions (Table 1, entries 1-4). The replacement of CsOAc with other additives resulted in a slightly lower yield (Table 1, entries 5-7). Further investigation of solvents revealed that the reaction could be carried out only with the participation of alcohol solvents, while DCM, THF, 1,4-dioxane, and PBS buffer (PB) essentially gave no product formation (Table 1, entries 14-17).

Table 1. Optimization of Reaction Conditions.

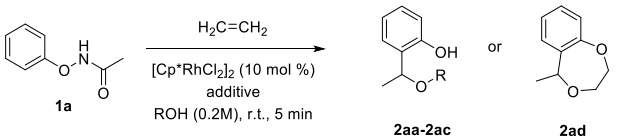

Entry	Catalyst	Additive (equiv)	Solvent	% Yield
1	$[Cp^*IrCl_2]_2$	CsOAc (1.0)	MeOH	ND
2	$[Ru(pcymene)Cl_2]_2$	CsOAc (1.0)	MeOH	ND
3	$Ru(COD)Cl_2$	CsOAc (1.0)	MeOH	ND
4	$[Pt(NH_3)_2Cl_2]$	CsOAc (1.0)	MeOH	ND
5	$[Cp^*RhCl_2]_2$	K_2CO_3 (1.0)	MeOH	**2aa** (68)
6	$[Cp^*RhCl_2]_2$	Na_2CO_3 (1.0)	MeOH	**2aa** (65)
7	$[Cp^*RhCl_2]_2$	CsOPiv (1.0)	MeOH	**2aa** (64)
8	$[Cp^*RhCl_2]_2$	CsOAc (0.5)	MeOH	**2aa** (70)
9	$[Cp^*RhCl_2]_2$	CsOAc (1.0)	MeOH	**2aa** (87)
10	$[Cp^*RhCl_2]_2$	CsOAc (2.0)	MeOH	**2aa** (82)
11	$[Cp^*RhCl_2]_2$	CsOAc (1.0)	EtOH	**2ab** (79)
12	$[Cp^*RhCl_2]_2$	CsOAc (1.0)	*n*-propanol	**2ac** (83)
13	$[Cp^*RhCl_2]_2$	CsOAc (1.0)	EG	**2ad** (68)
14	$[Cp^*RhCl_2]_2$	CsOAc (1.0)	DCM	ND
15	$[Cp^*RhCl_2]_2$	CsOAc (1.0)	THF	ND
16	$[Cp^*RhCl_2]_2$	CsOAc (1.0)	1,4-Dioxane	ND
17	$[Cp^*RhCl_2]_2$	CsOAc (1.0)	PB	ND
18	$[Cp^*RhCl_2]_2$	CsOAc (1.0)	MeOH: PB =1:9	**2aa** (57)
19	$[Cp^*RhCl_2]_2$	CsOAc (1.0)	EG: PB =1:9	**2ad** (63)

ND, not detected; EG, ethylene glycol; PBS buffer, PB; r.t., room temperature.

10.1002/anie.202108335

Under optimal conditions, the substrate scope of *N*-phenoxyacetamides was first investigated. As shown in Table 2, various *N*-phenoxyacetamides with *ortho*, *meta*, or *para* electron-neutral and electron-donating substituents such as CH_3 and OCH_3 groups (**2aa-2ad**, **2e**, **2f**, **2k**, **2i**, **2q,** and **2r**) afforded excellent selectivity and high yields. Electron-withdrawing functional groups (such as F, Cl, and Br) were well tolerated (**2b-2d**, **2h-2j,** and **2n-2p**), and the corresponding products were isolated in yields ranging from 73% to 88%. It is worth noting that the reaction of *N*-phenoxyacetamide substrates containing an electron-withdrawing trifluoromethyl group (**2g**, **2m,** and **2s**) resulted in poor yields (52%, 47, and 48%, respectively). In particular, the *meta*-substituents on *N*-phenoxyacetamides possessed good regioselectivity, and functionalization occurred mainly on the *ortho* C-H at the C-2 position (**2h-2m**).

Table 2. Scope of Rh-catalysed *ortho*-hydrocarbon activation.*

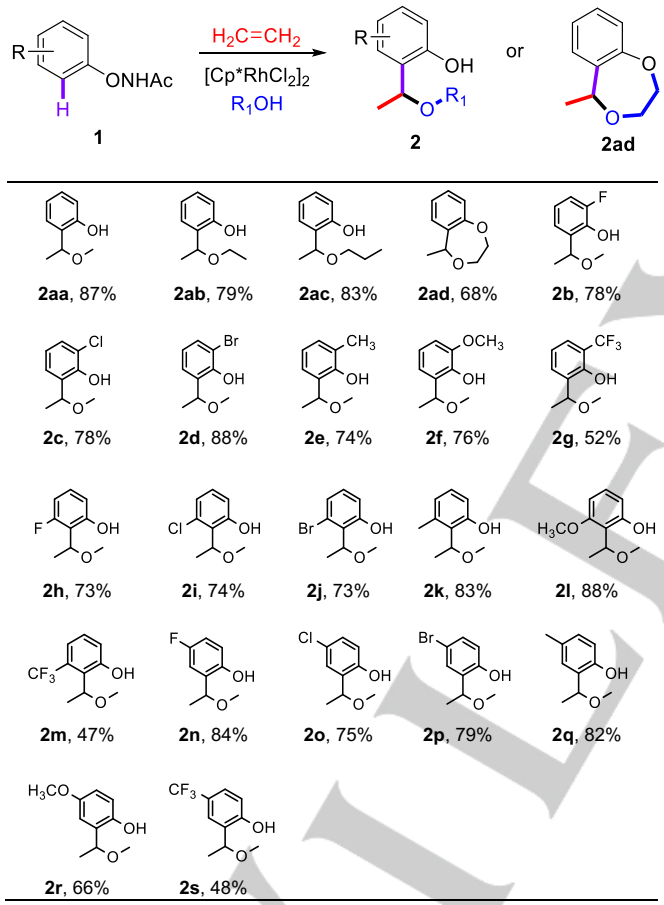

*Reaction conditions: 0.2 mmol of 1, 5 mL of ethylene, $[RhCp^*Cl_2]_2$ (10 mol%), 1.0 equiv of CsOAc in 0.2 M R_1OH at room temperature for 5 min.

We further designed and synthesized three fluorophore-tagged Rh(III)-based probes for the selective and quantitative detection of ethylene *in vivo*. In this report, we chose the Rh(III) metal complex (Moiety A Figure 1a) as the fluorescent response site and ethylene binding site because it meets the following requirements. First, the presence of rhodium could quench the fluorescence of the coumarin core via heavy metal atom electronic effects. Second, upon reacting with ethylene, a corresponding hydrocarbon activation reaction occurs to replace rhodium and generate a new fluorescent substance. Third, the Rh(III) cyclopentenyl complex possesses relatively high water solubility, which supports its direct application for ethylene sensing in complex biological systems. The preparation of these probes is very straightforward, and the route is shown in Figure 1b.

Various solvents were evaluated for dissolving probes to detect ethylene, including dimethyl sulfoxide (DMSO), PBS buffer (PB), dichloromethane (DCM), ethyl acetate (EA), 1,4-dioxane (1,4-Diox), dimethyl formamide (DMF), tetrahydrofuran (THF), acetonitrile (ACN), methanol (CH_3OH) + PB, ethanol (EtOH) + PB, *n*-propanol (NPA) + PB, *n*-butanol (NBA) + PB, and ethylene glycol (EG) + PB. As shown in Figure S3, adequate ethylene gas was injected into different probe solutions, and no significant fluorescence intensity changes were observed upon the application of any of these organic solvents except the alcohol solvents. However, when alcohol solvents were used as part of the reaction solvent, the reaction system would release a stronger fluorescent species upon exposure to ethylene gas, which illustrated that the solvent plays an extremely important role in the detection performance of the fluorescence probes.

To further clarify the mechanism of the reaction between the probe and ethylene, ^1H NMR titration experiments were performed in methanol-d_4 solvent. As shown in Figure S4, the chemical shifts at 6.16, 7.84, 7.21, 6.81, 2.21, and 1.67 ppm were assigned to the H_1~H_6 protons of **CEP-1**, respectively. The **CEP-1** solution was injected with different volumes of ethylene gas for 2 min, and as the volume of ethylene increased, the intensity of the hydrogen proton signals belonging to **CEP-1** disappeared gradually; meanwhile, a new set of peaks (δH_1' = 6.08 ppm, δH_2' = 7.79 ppm, δH_3' = 7.33 ppm, δH_4' = 6.74 ppm, δH_5' = 5.19 ppm, δH_6' = 1.56 ppm) appeared, which indicated that a chemical reaction occurred between **CEP-1** and ethylene to generate new substances. The ^1H and ^{13}C NMR spectrum of the separated fluorescent substance also showed the transformation of **CEP-1** to **CEP-1-ETa** (Figure S35). While performed in methanol-d_4 solvent, the ^1H and ^{13}C NMR spectrum lacked a methyl peak with chemical shift of approximately 3.14 ppm and 56.4 ppm (Figure S36), respectively, proving that the methanol solvent not only acted as a solvent but also participated in the reaction. In addition, 50 mM CH_3OH, EtOH, *n*-propanol, *n*-butanol, and ethylene glycol were utilized to dissolve **CEP-1** and generate various fluorescent substances to detect ethylene (Figure 1c).

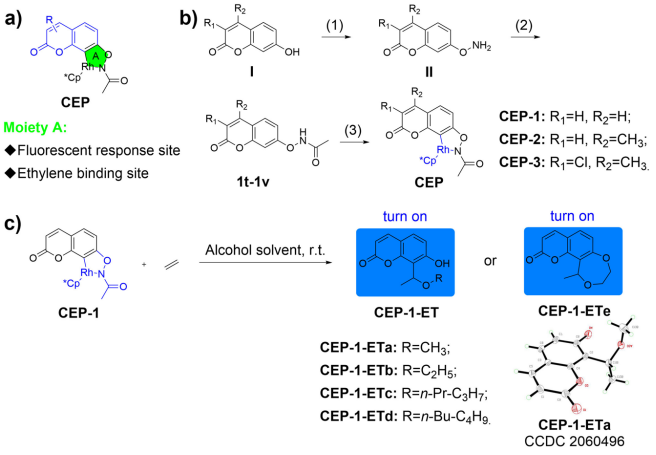

Figure 1. Preparation of the fluorophore-tagged Rh(III)-based probes. a) Diagram of the design of fluorescent probes with moiety A as the fluorescent

response site and ethylene binding site. b) Synthetic route of **CEP**. Reagents and conditions: (1) NaH, *O*-(mesitylsulfonyl)hydroxylamine, DMF; (2) Ac_2O, DCM; (3) $[Cp^*RhCl_2]_2$, K_2CO_3, CH_3CN. c) Chemical structure of fluorescent substance after injecting excess ethylene into **CEP-1** dissolved in different alcohol solvents (CH_3OH, EtOH, *n*-propanol, *n*-butanol, and ethylene glycol) and diagram illustrating turn-on with **CEP-1** in the presence of ethylene.

Next, a series of **CEP-1** concentration systems were evaluated to determine the best response of **CEP-1** to ethylene. In line with the change in fluorescence intensity before and after the addition of ethylene for 2 min to different concentrations of the **CEP-1** solution, we finally chose 100 μM as the optimal **CEP-1** concentration (Figure 2a). Additionally, the absorption spectra of **CEP-1** in PBS buffer solution (100 μM, pH = 7.3, containing 10% ethylene glycol) with ethylene were investigated. Figure 2b shows an absorption maximum at 340 nm for the **CEP-1** solution alone; however, new absorption bands emerged at 368 nm and 328 nm after the addition of ethylene for 2 min, indicating that a chemical reaction occurred between **CEP-1** and ethylene, which is consistent with the ^{1}H NMR results (Figure S4). Besides, time-dependent reaction kinetic experiment showed that **CEP-1** reacts with ethylene very rapidly, and the fluorescence intensity reached the maximum within 2 minutes after the addition of 2 mL ethylene (Figure 2c).

With these findings in mind, we continued to evaluate the ability of the probes to detect various concentrations of ethylene gas. This was done by injecting ethylene into solutions of different probes (100 μM, pH = 7.3, containing 10% ethylene glycol) via a gastight syringe and measuring the fluorescence intensity after 2 min (Figure 2d, Figure S5 and S6). A good linear correlation was observed between the fluorescence intensity at 460 nm and the volume of ethylene in the range of 10-250 μL. The limits of detection (LODs) for ethylene were calculated to be 0.29 μL for **CEP-1**, 0.34 μL for **CEP-2** and 0.49 μL for **CEP-3** based on the IUPAC definition (CDL = 3σ/k),[19] which correspond to 52 ppb, 60 ppb, and 88 ppb, respectively, in the headspace of the sample bottle. These values are low enough to detect the <1 ppm levels of ethylene commonly found in many biological samples during ripening.[20] As shown in Table S1, among the three **CEPs**, **CEP-1** displayed the best optical properties with the highest molar extinction coefficient (1.04 M^{-1} cm^{-1}) and fluorescence quantum yields (0.79) when reacted with ethylene. In addition, compared with other previously published fluorophore-tagged Grubbs-Catalyst-Based ethylene probes, **CEP-1** shows obvious advantages in detection limit, response time, selectivity and Stokes shift, except the relatively short emission wavelength (Table S2). Thus, we decided to utilize **CEP-1** for further investigation.

Subsequently, the response of **CEP-1** to ethylene was detected at pH values of 2 to 12 in a mixture of EG/H_2O (1/9) solution. As shown in Figure 2e, **CEP-1** (100 μM, containing 10% ethylene glycol) itself exhibited no fluorescence in this pH range, while after the addition of ethylene (2 mL) for 2 min, the strongest fluorescence intensity appeared in the pH range of 6 to 12, which was within the normal physiological range. These results indicated that **CEP-1** has potential applications for the detection of ethylene in biological samples.

To verify the selectivity of **CEP-1** for ethylene, studies were conducted in the presence of glutathione and other competitive unsaturated plant metabolite molecules, including farnesol, citronellol, limonene, myrcene, pinene, and terpinolene. As illustrated in Figure 2f, the addition of ethylene (2 mL) induced a strong fluorescence enhancement, whereas other tested interferents did not trigger an apparent fluorescence enhancement. This result indicated that **CEP-1** displayed excellent selectivity towards ethylene and was suitable for detecting ethylene in biological samples.

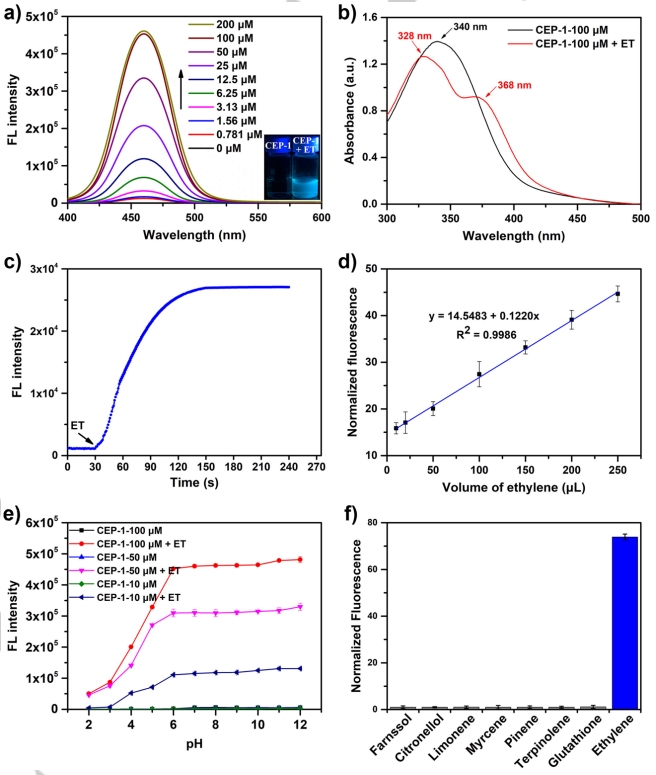

Figure 2. Spectral characterization and selectivity of **CEP-1**. a) Fluorescence intensity changes of different concentrations of **CEP-1** (0-200 μM, λ_{ex} = 365 nm) in the presence of excess ethylene in a mixed EG/PB (v/v = 1/9) solvent. The inset shows the fluorescence change of **CEP-1** (100 μM). b) Absorption spectra of **CEP-1** (100 μM) in the absence and presence of excess ethylene in EG/PB (v/v = 1/9). c) Time-based monitoring of **CEP-1** (100 μM) exposed to a theoretical concentration of 2 mL of ethylene (957 mM) dissolved in EG/PB (v/v = 1/9). λ_{ex} = 365 nm/λ_{em} = 460 nm. d) Fluorescence intensity of **CEP-1** (100 μM) as a function of the ethylene gas volume in EG/PB (v/v = 1/9) solvent. λ_{ex} = 365 nm/λ_{em} = 460 nm. End points represent normalized fluorescence after the addition of ethylene for 2 min. e) pH dependence of the **CEP-1**-ethylene system at different pH conditions in EG/PB (v/v = 1/9). λ_{ex} = 365 nm/λ_{em} = 460 nm. f) Selectivity study of **CEP-1** (100 μM) against glutathione and various types of terpenes (6 mM). λ_{ex}= 365 nm/λ_{em} = 460 nm. The data shown are the average of four independent experiments. Error bars denote SD.

The encouraging *in vitro* results prompted us to determine whether **CEP-1** could be applied to visualize ethylene in live cells using confocal fluorescence microscopy. The cytotoxicity of **CEP-1** before or after treated with ethylene was evaluated with a CCK-8 assay, which was performed on CHO-K1 cells incubated with **CEP-1** at different concentrations (0, 1, 2, 4, 6, 8, 10 μM) for 12 h. The CCK-8 results indicated that the cell viability of the treatments with or without ethylene were both higher than 80% even after incubation with 10 μM **CEP-1** (EG/PB = 1/9) for 12 h, suggesting almost negligible cytotoxicity of **CEP-1** and its reaction products to living CHO-K1 cells (Figure S42). Then, **CEP-1** was tested for its ability to visualize changes in ethylene levels in live cells. CHO-K1 cells were incubated with 10 μM **CEP-1** for 15 min at 37 °C,

leading to almost no fluorescence. However, when living CHO-K1 cells were treated with ethylene gas (0.5 mL and 2 mL, respectively) for 30 min, and then incubated with **CEP-1** (10 μM) at 37 °C under 5% CO_2 for another 30 min and imaged washing with PBS, a prominent blue fluorescence response was observed (Figure 3a). Flow cytometry was used to quantify the fluorescence intensity of CHO-K1 cells. It is obvious that the ethylene and **CEP-1** co-treated CHO-K1 cells show much higher fluorescence signals than only **CEP-1** treated cells (Figure 3c), which is consistent with the fluorescence intensity measured by ImageJ software (Figure 3b). These results indicated that **CEP-1** has good cell permeability and low toxicity and can be exploited for cell imaging and the rapid detection of ethylene *in vivo*.

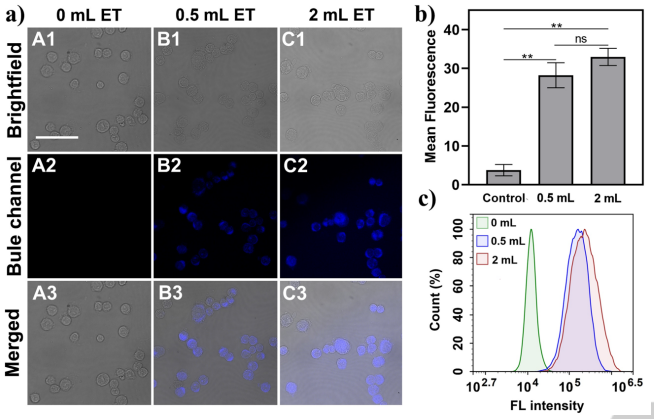

Figure 3. Visualization of ethylene in live cells using **CEP-1**. a) Confocal microscopy images of ethylene detection in live CHO-K1 cells incubated with 10 μM **CEP-1** for 30 min in the (A) absence and (B and C) presence of ethylene (injected with 0, 0.5, 2 mL of ethylene for 30 min): (1) brightfield; (2) bule channel; (3) merged. Scale bars, 100 μm. The images were collected at 410-480 nm (blue channel) upon excitation at 405 nm. b) Normalized mean fluorescence intensities extracted from ROIs using the ImageJ software. Plotted data are the average of three independent experiments. Each experiment was repeated for three times. Three fields (290.62 μm × 290.62 μm, 15 cells of each field) of view per replicate were measured. Error bars denote ± SD. Statistical analysis was performed using one-way ANOVA with Tukey's multiple comparisons test. **P < 0.002, ns = not significant. c) Flow cytometry analysis of CHO-K1 cells were pre-treated with 0, 0.5, 2 mL of ethylene for 30 min and then incubated with 10 μM **CEP-1** for 30 min. Set the excitation wavelength at 405 nm and collect the fluorescence signals at 445/45 nm.

We further investigated the capacity of **CEP-1** to detect changes in endogenous ethylene levels in live plant samples. Considering that ACC is the immediate precursor of ethylene and is often used to elevate ethylene biosynthesis in plant, we selected ACC to enhance ethylene production. As shown in Figure S43a, two-month-old tobacco leaves were incubated with ACC for 12 h, and then the tobacco leaves were treated with 10 μM **CEP-1** (EG/PB = 1/9) for 30 min before imaging. As quantified in Figure S43b, no fluorescence enhancement was observed in tobacco leaves incubated with deionized water or ACC (1 mM) only. The tobacco leaves incubated with the **CEP-1** (10 μM) had weak fluorescence, suggesting that **CEP-1** could detect basal-level ethylene produced in tobacco leaves. In addition, a large fluorescence enhancement was observed when the tobacco leaves were pretreated with ACC for 12 h followed by treatment with **CEP-1** for 30 min.

To further confirm the applicability of **CEP-1** in detecting ethylene in the plant samples, the model plant *Arabidopsis thaliana* was tested. As shown in Figure 4a, leaf epidermal peels from old *A. thaliana* plants were subjected to local treatment with ethylene precursor (ACC) for plant ethylene accumulation. As quantified in Figure 4b, the levels of ethylene produced in the epidermal peels via ACC treatment were significantly higher than those produced in untreated leaf peels of *A. thaliana.* In addition, we used **CEP-1** to detect time-dependent ethylene production in leaf peels of *A. thaliana* (Col-0) plants subjected to a 12 h stimulant (ACC) treatment. Confocal microscopy imaging shows that leaf peels fluorescence increased in a time-dependent manner within 30 minutes after treated with **CEP-1** (Figure 4c and 4d). These data are consistent with literature reports that have shown consistently triggered ethylene gas production in Col-0 plants after ACC exposure.[21]

To demonstrate the sensitivity of **CEP-1** to detect endogenous differences in ethylene production, we applied our strategy to measure systemic ethylene gas accumulation in two mutants, *acs2/6/4/5/9* and *4myc-ACS6^{DDD}*. The mutant *acs2/6/4/5/9*, which contains knock outs of five functional ACS genes, produced much lower levels of ethylene during pathogen infection.[22] The mutant *4myc-ACS6^{DDD}* is a phosphor-mimicking form.[23] Compared with wild-type Col-0, a knockout *acs2/6/4/5/9* that has a reduced capacity to generate ethylene during plant immune response, showed no significant fluorescent change after **CEP-1** addition (Figure 5a and 5c). In contrast, the phosphor-mimicking *4myc-ACS6^{DDD}* exhibited a significant increase in fluorescence compared to wild-type Col-0 (Figure 5b and 5c). These findings demonstrated that the measured endogenous ethylene levels are directly linked to endogenous ethylene production and that the developed method could be used to characterize different mutants with altered ethylene levels.[22, 24]

10.1002/anie.202108335

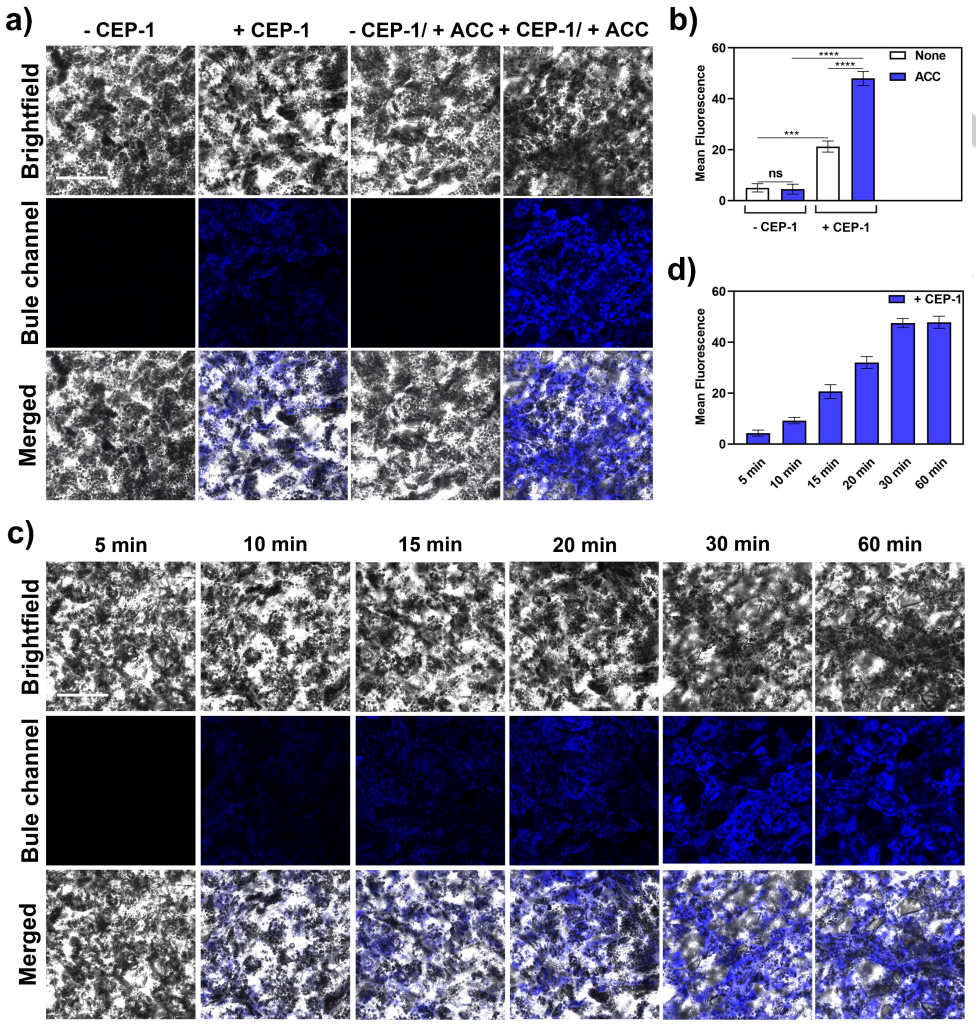

Figure 4. Detection of ethylene generated in *A. thaliana* plants. a) Fluorescence and brightfield imaging of ethylene detection in *A. thaliana* plants subjected to a 12 h stimulant (ACC) treatment. Scale bars, 100 μm. b) Normalized mean fluorescence intensities of *A. thaliana* plants with ACC treatment. c) Time-dependent detection of ethylene in *A. thaliana* plants subjected to a 12 h stimulant (ACC) treatment. Scale bars, 100 μm. d) Normalized mean fluorescence intensities of time-dependent detection of ethylene in *A. thaliana* plants with ACC treatment. Plotted data are the average of three independent experiments. Each experiment was repeated for three times. Mean fluorescent intensity was measured from five individual leaf peels (fifteen regions in random, 290.62 μm × 290.62 μm of each region) using ImageJ software. Error bars denote ± SD. ***P < 0.0002, ****P < 0.0001, ns = not significant.

10.1002/anie.202108335

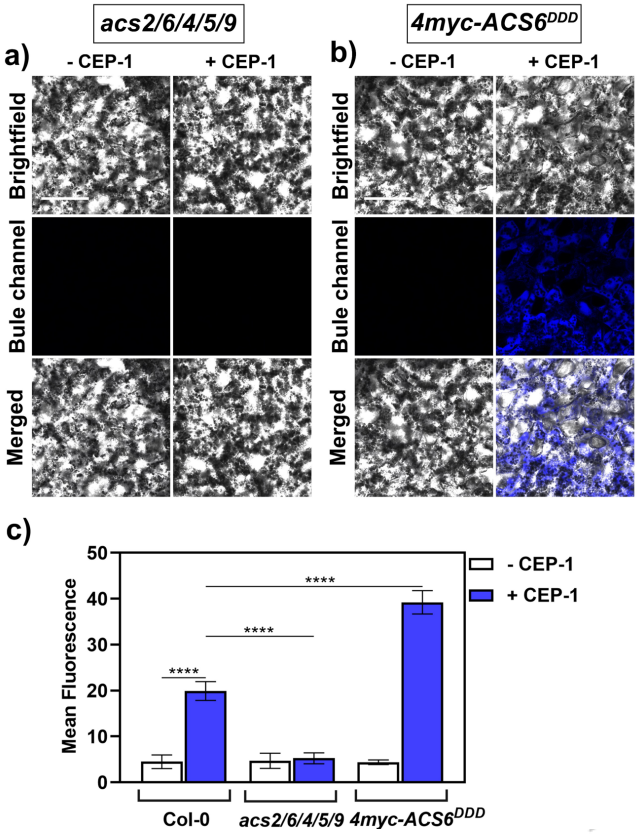

Figure 5. Detection of ethylene produced in *A. thaliana* mutants. a) Fluorescence and brightfield imaging of epidermal peels applied with **CEP-1** (10 μM) to the ethylene biosynthesis-defective *acs2/6/4/5/9* and b) the phosphor-mimicking *4myc-ACS6^{DDD}*. Scale bars, 100 μm. c) Quantification of the imaging data (a and b). Plotted data are the average of three independent experiments. Each experiment was repeated for three times. Mean fluorescent intensity was measured from five individual leaf peels (fifteen regions in random, 290.62 μm × 290.62 μm of each region) using ImageJ software. Error bars denote ± SD. Statistical analysis was performed using one-way ANOVA with Tukey's multiple comparisons test. ****P < 0.0001. Error bars are ± SD (n = 15).

Plant innate immunity system triggered by perception of Pathogen/Microbe associated molecular patterns (P/MAMPs) is considered to be the first barrier to resistance the invasion of pathogens or microbes. P/MAMPs can activate pattern-recognition receptors (PRRs), which in turn initiate a variety of downstream signalling events leading to the activation of a basal resistance that is referred to P/MAMP-triggered immunity (PTI/MTI). For instance, bacterial flagellin and NLPs (necrosis and ethylene-inducing peptide 1 like proteins) are recognized by pattern recognition receptors (PRRs) and to activate antimicrobial defences. Which are usually linked with the ethylene biosynthesis, accumulation of reactive oxygen species (ROS), cell wall cross-linking and the release of secondary metabolites.[25] Depicted in Figure 6a, flg22 is composed of a 22-amino acid sequence and could induce plant defence mechanisms to produce more ethylene; and nlp20 is a conserved 20-amino acid fragment that could also result in immune activation to produce more ethylene by cytotoxic and noncytotoxic NLPs.[26] As shown in Figure 6b, we tested leaf epidermal peeled from old *A. thaliana* plants subjected to local treatment with P/MAMP for plant ethylene accumulation. As quantified in Figure 6c, the levels of ethylene produced in the epidermal peels after P/MAMP treatment were significantly higher than those produced in untreated epidermal peels of *A. thaliana*. These data are similar to the reported results of triggered ethylene biosynthesis in Col-0 plants after flg22 or nlp20 exposure.[26b]

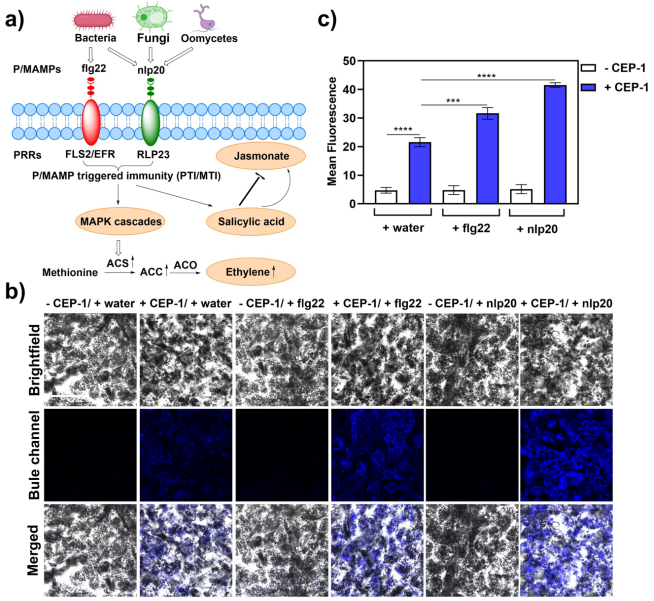

Figure 6. Leaves of *A. thaliana* imaging of ethylene accumulation in response to P/MAMP (flg22 or nlp20). a) Schematic overview of the general pathway that leads to PTI/MTI response. b) Fluorescence and brightfield images of ethylene detection in *A. thaliana* plants subjected to a 12 h P/MAMP (flg22 or nlp20) treatment. Scale bars, 100 μm. c) Normalized mean fluorescence intensities of *A. thaliana* plants with P/MAMP treatment. Plotted data are the average of three independent experiments. Each experiment was repeated for three times. Mean fluorescent intensity was measured from five individual leaf peels (fifteen regions in random, 290.62 μm × 290.62 μm of each region) using ImageJ software. Error bars denote ± SD. Statistical analysis was performed using one-way ANOVA with Tukey's multiple comparisons test. ***P < 0.0002, ****P < 0.0001. Error bars are ± SD (n = 15).

Conclusion

In summary, three fluorophore-tagged Rh(III)-based probes were developed for the selective and quantitative detection of ethylene. Quantitative analysis indicated that **CEP-1** possessed the highest sensitivity with a limit of detection of 52 ppb ethylene in air. Moreover, **CEP-1** exhibited high selectivity of ethylene and avoided interference from other competing unsaturated molecules of plant metabolites. Furthermore, we demonstrated that **CEP-1** has the potential to detect endogenous ethylene gas not only in living CHO-K1 cells (in the presence of exogenously added ethylene) but also endogenous ethylene produced in tobacco and *A. thaliana* plants. These fluorophore-tagged Rh(III)-based probes provide a novel reaction mechanism for the spatial real-time monitoring of endogenous ethylene in cells and plant leaves. We expect that **CEP-1** could serve as an effective tool for better understanding of the regulation of ethylene biosynthesis and ethylene signal transduction in living biological systems and thus promote the ethylene-related physiological research in plants.

Acknowledgements

The authors would like to thank Prof. Xiaorong Tao and Prof. Suomeng Dong of Nanjing Agricultural University for helpful discussions and insightful comments on the manuscript. This work was financially supported by the National Key Research and Development Program of China (2017YFD0200500 and 2018YFD0200100), the National Natural Science Foundation of China (32072443) and Natural Science Foundation of Jiangsu Province (BK20201323).

Conflict of interest

The authors declare no conflict of interest.

Keywords: bioimaging • hydrocarbon activations • fluorescent probes • ethylene

[1] a) M. E. Saltveit, *Postharvest Biol. Technol.* **1999**, *15*, 279-292; b) T. T. Storch, T. Finatto, M. Bruneau, M. Orsel-Baldwin, J. P. Renou, C. V. Rombaldi, V. Quecini, F. Laurens, C. L. Girardi, *J. Agric. Food Chem.* **2017**, *65*, 7813-7826; c) J. H. Zhang, D. Cheng, B. B. Wang, I. Khan, Y. H. Ni, *J. Agric. Food Chem.* **2017**, *65*, 7308-7319; d) Y. D. Liu, M. F. Tang, M. C. Liu, D. D. Su, J. Chen, Y. S. Gao, M. Bouzayen, Z. G. Li, *Small Methods* **2020**.

[2] S. F. Yang, N.E. Hoffman, *Annu. Rev. Plant Physiol.* **1984**, *35*, 155-189.

[3] B. M. Binder, *J. Biol. Chem.* **2020**, *295*, 7710-7725.

[4] M. Santiago Cintrón, O. Green, J. N. Burstyn, *Inorg. Chem.* **2012**, *51*, 2737-2746.

[5] H. Pham-Tuan, J. Vercammen, C. Devos, P. Sandra, *J. Chromatogr. A* **2000**, *868*, 249-259.

[6] a) F. J. M. Harren, J. Mandon, S. M. Cristescu, in *Encyclopedia of Analytical Chemistry*, **2012**; b) S. M. Cristescu, J. Mandon, D. Arslanov, J. De Pessemier, C. Hermans, F. J. M. Harren, *Ann. Bot.* **2013**, *111*, 347-360.

[7] a) M. A. G. Zevenbergen, D. Wouters, V. A. T. Dam, S. H. Brongersma, M. Crego-Calama, *Anal. Chem.* **2011**, *83*, 6300-6307; b) B. Esser, J. M. Schnorr, T. M. Swager, *Angew. Chem., Int. Ed.* **2012**, *51*, 5752-5756.

[8] O. Green, N.A. Smith, A.B. Ellis, J. N. Burstyn, *J. Am. Chem. Soc.* **2004**, *126*, 5952-5953.

[9] B. Esser, T. M. Swager, *Angew. Chem., Int. Ed. Engl.* **2010**, *49*, 8872-8875.

[10] Y. Hitomi, T. Nagai, M. Kodera, *Chem. Commun. (Camb)* **2012**, *48*, 10392-10394.

[11] a) F. H. Hu, Z. X. Chen, L. Y. Zhang, Y. H. Shen, L. Wei, W. Min, *Angew. Chem., Int. Ed.* **2015**, *54*, 9821-9825. b) S. Benson, A. Fernandez, N. D. Barth, F. de Moliner, M. H. Horrocks, C. S. Herrington, J. L. Abad, A. Delgado, L. Kelly, Z. Y. Chang, Y. Feng, M. Nishiura, Y. Hori, K. Kikuchi, M. Vendrell, *Angew. Chem., Int. Ed.* **2019**, *58*, 6911-6915. c) F. de Moliner, K. Knox, D. Gordon, M. Lee, W. J. Tipping, A. Geddis, A. Reinders, J. M. Ward, K. Oparka, M. Vendrell, *Angew. Chem., Int. Ed.* **2021**, *60*, 7637-7642.

[12] a) D. A. Iovan, S. Jia, C. J. Chang, *Inorg. Chem.* **2019**, *58*, 13546-13560. b) K. J. Bruemmer, S. W. M. Crossley, C. J. Chang, *Angew. Chem., Int. Ed.* **2020**, *59*, 13734-13762.

[13] S. N. W. Toussaint, R. T. Calkins, S. Lee, B. W. Michel, *J. Am. Chem. Soc.* **2018**, *140*, 13151-13155.

[14] M. T. Sun, X. Yang, Y. N. Zhang, S. H. Wang, M. W. Wong, R. Y. Ni, D. J. Huang, *J. Agric. Food Chem.* **2019**, *67*, 507-513.

[15] K. Vong, S. Eda, Y. Kadota, I. Nasibullin, T. Wakatake, S. Yokoshima, K. Shirasu, K. Tanaka, *Nat. Commun.* **2019**, *10*, 5746.

[16] P. P. Duan, X. Lan, Y. Chen, S. S. Qian, J. J. Li, L. Lu, Y. B. Lu, B. Chen, M. Hong, J. Zhao, *Chem. Commun. (Camb)* **2014**, *50*, 12135-12138.

[17] Y. Chen, D. Q. Wang, P. P. Duan, R. Ben, L. Dai, X. R. Shao, M. Hong, J. Zhao, Y. Huang, *Nat. Commun.* **2014**, *5*, 4610.

[18] Q. Wu, Y. Chen, D. Y. Yan, M. Y. Zhang, Y. Lu, W. Y. Sun, J. Zhao, *Chem. Sci.* **2017**, *8*, 169-173.

[19] a) S. Fernández-Alonso, T. Corrales, J. L. Pablos, F. Catalina, *Sens. Actuators, B* **2018**, *270*, 256-262; b) Z. Li, Y. Q. Xu, H. L. Zhu, Y. Qian, *Chem. Sci.* **2017**, *8*, 5616-5621.

[20] S. P. Burg, E. A. Burg, *Science* **1965**, *148*, 1190-1196.

[21] D. O. Adams, S. F. Yang, *Proc. Natl. Acad. Sci. U. S. A.* **1979**, *76*, 170-174.

[22] S. Li, X. F. Han, L. Y. Yang, X. X. Deng, H. J. Wu, M. M. Zhang, Y. D. Liu, S. Q. Zhang, J. Xu, *Plant, Cell Environ.* **2018**, *41*, 134-147.

[23] S. Joo, Y. D. Liu, A. Lueth, S. Q. Zhang, *Plant J.* **2008**, *54*, 129-140.

[24] Y. Fichman, G. Miller, R. Mittler, *Mol. Plant* **2019**, *12*, 1203-1210.

[25] a) C. M. J. Pieterse, A. Leon-Reyes, S. Van der Ent, S. C. M. Van Wees, *Nat. Chem. Biol.* **2009**, *5*, 308-316; b) X. Du, S. Wang, F. Gao, L. S. Zhang, J. H. Zhao, H. S. Guo, C. L. Hua, *Sci. China: Life Sci.* **2017**, *60*, 852-860; c) I. Albert, L. S. Zhang, H. Bemm, T. Nürnberger, *Mol. Plant-Microbe Interact.* **2019**, *32*, 1038-1046; d) F. Zhou, A. Emonet, V. Denervaud Tendon, P. Marhavy, D. S. Wu, T. Lahaye, N. Geldner, *Cell* **2020**, *180*, 440-453 e418.

[26] a) S. Oome, T. M. Raaymakers, A. Cabral, S. Samwel, H. Böhm, I. Albert, T. Nürnberger, G. Van den Ackerveken, *Proc. Natl. Acad. Sci. U. S. A.* **2014**, *111*, 16955-16960; b) I. Albert, H. Böhm, M. Albert, C. E. Feiler, J. Imkampe, N. Wallmeroth, C. Brancato, T. M. Raaymakers, S. Oome, H. Q. Zhang, E. Krol, C. Grefen, A. A. Gust, J. J. Chai, R. Hedrich, G. Van den Ackerveken, T. Nürnberger, *Nat. Plants* **2015**, *1*, 15140.

10.1002/anie.202108335

WILEY-VCH

RESEARCH ARTICLE

Entry for the Table of Contents

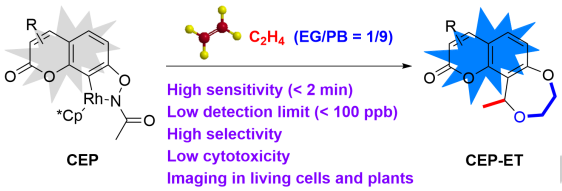

Fluorophore-tagged Rh(III)-based fluorogenic probes (see picture) were developed for rapid (< 2 min), highly selective, and quantitative detection of ethylene. Additionally, we demonstrated that **CEP-1** has the capacity to detect endogenous ethylene gas in living cells and plants.